Research Square

Preprints are preliminary reports that have not undergone peer review.
They should not be considered conclusive, used to inform clinical practice,
or referenced by the media as validated information.

Spatial trapping and anteroposterior segregation of the default mode network in schizophrenia

Jesús Martín-Fernández

jesusmarfdez9@gmail.com

Hospital Universitario Nuestra Señora de Candelaria

Nayra Caballero-Estebaranz

Hospital Universitario Nuestra Señora de Candelaria

Pedro Barreiro-Marín

Hospital Universitario Nuestra Señora de Candelaria

Julián Portero-Navarro

Hospital Universitario Nuestra Señora de Candelaria

Óscar Pérez Díaz

Hospital Universitario Nuestra Señora de Candelaria

Marta González Puga

Hospital Universitario Nuestra Señora de Candelaria

Estefanía Hernández-Martín

Hospital Universitario Nuestra Señora de Candelaria

Francisco Rodríguez-Pulido

Universidad de La Laguna

Article

Keywords: schizophrenia, default mode network, brain modes, spatial trapping, co-participation

Posted Date: November 18th, 2026

DOI: https://doi.org/10.21203/rs.3.rs-11525287/v1

License: This work is licensed under a Creative Commons Attribution 4.0 International License.
Read Full License

Additional Declarations: No competing interests reported.

Spatial trapping and anteroposterior segregation of the default mode network in schizophrenia

Jesús Martín-Fernández, MD[1,2,3*]; Nayra Caballero Estebaranz, PhD[1,2,4]; Pedro Barreiro Marín, PhD[5]; Julián Portero Navarro, PhD[6]; Óscar Pérez Díaz, PhD[1,4]; Marta González Puga, PhD[5]; Estefanía Hernández-Martín, PhD[1,3,4] ; Francisco Rodríguez Pulido, PhD[,2,7]

1. Department of Awake Cognitive Mapping (UNCOG), Hospital Universitario Nuestra Señora de Candelaria, Tenerife, Spain.
2. Canary Association of Creative Therapies (ASCATEC), Tenerife, Spain.
3. Department of Cognitive-affective neuroscience, e-Awake Institute, Tenerife, Spain
4. Fundación Canaria Instituto de Investigación Sanitaria de Canarias (FIISC), Santa Cruz de Tenerife, Spain.
5. Department of Psychiatry, Hospital Universitario Nuestra Señora de Candelaria, Tenerife, Spain.
6. Department of Radiology, Neuroradiology section, Hospital Universitario Nuestra Señora de Candelaria, Tenerife, Spain.
7. Department of Psychiatry, Medical school, University of La Laguna, Spain

Running title: Modal organisation in schizophrenia

Correspondence to: Jesús Martín-Fernández, MD.

Email: jesusmarfdez9@gmail.com.

Abstract

The spatial organisation of the default mode network (DMN) across recurrent brain configurations remains poorly understood in schizophrenia. Here, we introduce two indices to quantify how selectively a network is represented across brain modes and whether selected anterior and posterior regions participate in the same configurations.

Resting-state functional MRI from 16 healthy controls and 11 participants with non-acute schizophrenia was used to assess static and dynamic functional connectivity, global synchronisation, intrinsic ignition and variability measures. Leading Eigenvector Dynamics Analysis identified the brain modes. The Spatial Trapping Index (STI) measured the distribution of relative network composition across four modes, while anterior–posterior co-participation (CAP) measured shared these modes. The two indices were compared using permutation test within Holm correction.

Static functional connectivity was lower within the dorsal attention network, while dynamic functional connectivity showed greater variability in several network. No significant differences were detected in global synchronisation, intrinsic ignition or the three signatures of metastability. Mean DMN composition was similar between groups, but STI was higher in SCZ, while CAP was lower. Bootstrap resampling retained the observed directions in 89.6% of STI contrasts and 91.9% of CAP contrasts.

These findings suggest that DMN representation is less selective across brain modes in schizophrenia, while selected anterior and posterior regions participate less consistently together. STI and CAP offer a new way to quantify these complementary aspects of spatial organisation, providing a basis for investigating their clinical relevance.

Keywords: schizophrenia; default mode network; brain modes; spatial trapping; co-participation

Abbreviated summary: The authors found less selective default mode network representation across brain modes and lower medial anterior–posterior co-participation in schizophrenia. The two spatial indices distinguish network representation from regional assembly.

1. Introduction

The brain's repertoire of spatiotemporal activity patterns in schizophrenia remains a topic of ongoing research interest. Friston disconnection hypothesis links abnormal regulation of synaptic efficacy to disturbed integration among specialised neuronal systems, although a primary pathological locus has not been established [1][2]. A multilevel, complex-systems account relates local neuronal dynamics to collective activity emerging through distributed interactions; coupling, transmission delays and fluctuations jointly shape the configurations that the system expresses [3][4]. Consequently, the anatomical distribution of an imaging abnormality does not, by itself, identify a unique site or mechanism of origin. An important objective is therefore to understand how coordination between brain regions gives rise to recurring whole-brain patterns and how their organisation differs in schizophrenia. These patterns, referred to here as brain states or modes, represent characteristic configurations of functional relationships between regions that reappear over time as brain activity evolves [5] [6] .

These recurring patterns can be studied by measuring how closely brain regions synchronise, how widely activity is integrated following regional events, and how coordination varies over time [7][8]. Measures of phase synchronisation and event-associated integration, termed intrinsic ignition, characterise aspects of collective activity, while metastability provides a framework for understanding intrinsically transient coordination [8][9]. In schizophrenia, synchronisation and metastability measures have been used to investigate disturbances in collective brain dynamics [7] [10]. However, global measures alone do not reveal which networks contribute to each pattern or which regions participate together. Similar overall levels of synchronisation or integration may therefore coexist with different spatial arrangements of brain activity. Therefore, an open question is how functional networks are represented across recurring brain modes and whether their constituent regions consistently participate in the same configurations.

Addressing this question requires identifying recurring whole-brain patterns and examining which functional networks contribute to each of them. Leading Eigenvector Dynamics Analysis (LEiDA) provides this approach by detecting recurrent configurations of phase alignment between regional blood oxygen level-dependent (BOLD) signals [5]. In healthy adults, Vohryzek et al., identified a globally coherent state and four configurations preferentially associated with the default mode, frontoparietal, visual and ventral attention networks [6]. These findings provide a basis for examining whether a network is mainly represented in particular modes or distributed more broadly across several configurations.

Among these networks, the default mode network (DMN) is of particular interest because schizophrenia has been associated with changes in both its connectivity and its participation in recurring brain states. Woodward et al., reported altered separation between default mode and executive regions despite no detectable difference in average connectivity within the DMN [11]. Other studies described weaker interactions among DMN subsystems and differences in anterior–posterior connectivity that depended on the brain state [12] [13]. Kottaram et al., also found changes in how frequently DMN-related configurations occurred, how long they persisted and how transitions between them unfolded [14]. Together, these findings motivate examining the spatial organisation of DMN participation: whether its representation is concentrated in particular modes or distributed across several, and whether its regions participate in those modes together.

Whether DMN regions participate together is particularly relevant to the relationship between its anterior and posterior components. Andrews-Hanna et al., identified a midline core comprising anterior medial prefrontal and posterior cingulate regions, linked to distinct DMN subsystems and involved in evaluating the personal and emotional significance of self-related information [15]. Together with evidence of autobiographical memory impairment in schizophrenia [16], this organisation motivates examining whether selected medial anterior regions and the posterior cingulate participate in the same recurring brain configurations.

These questions concern two distinct aspects of network organisation. First, the DMN may have a similar average representation in two groups while appearing mainly in one or two modes in one group and more evenly across several modes in the other. Second, this distribution does not reveal whether its anterior and posterior regions participate together, as different subsets of regions may represent the network in different configurations. We developed two complementary indices to distinguish these arrangements. The Spatial Trapping Index (STI) quantifies the effective number of modes across which a network's relative spatial representation is distributed [17]. The anterior–posterior modal co-participation index (CAP) uses Dice's similarity coefficient to assess shared modes between selected medial anterior regions and the posterior cingulate [18].

Here, we determine whether the spatial organisation of the DMN across recurrent whole-brain modes differs between healthy controls and participants with non-acute schizophrenia. We examined how DMN representation is distributed across modes and whether selected medial anterior regions and the posterior cingulate participate in the same configurations.

2. Results

2.1. Static and dynamic connectivity within and between networks

Static connectivity showed a mixed pattern of increases and decreases in SCZ relative to HC (Fig. 1A). The largest positive differences involved SAN–DMN ($\Delta z = 0.111$), SM–DMN ($\Delta z = 0.106$), and SM–FPN ($\Delta z = 0.060$). The largest reductions occurred within DAN ($\Delta z = -0.132$; $p<0.05$) and between VIS and DAN ($\Delta z = -0.084$; $p>0.05$). Within-DMN connectivity was similar between groups (HC, $r = 0.478$; SCZ, $r = 0.480$; $p>0.05$).

Dynamic connectivity variability was higher in SCZ across all network blocks (Fig. 1B). Six comparisons reached the statistics signification ($p<0.05$): within VIS ($\Delta = 0.031$) and between VIS–LIM ($\Delta = 0.029$), SM–LIM ($\Delta = 0.028$), DAN–LIM ($\Delta = 0.028$), SAN–LIM ($\Delta = 0.031$), and LIM–FPN ($\Delta = 0.026$). Five of these six comparisons involved the limbic network. The remaining comparisons did not reach the significance ($p>0.05$).

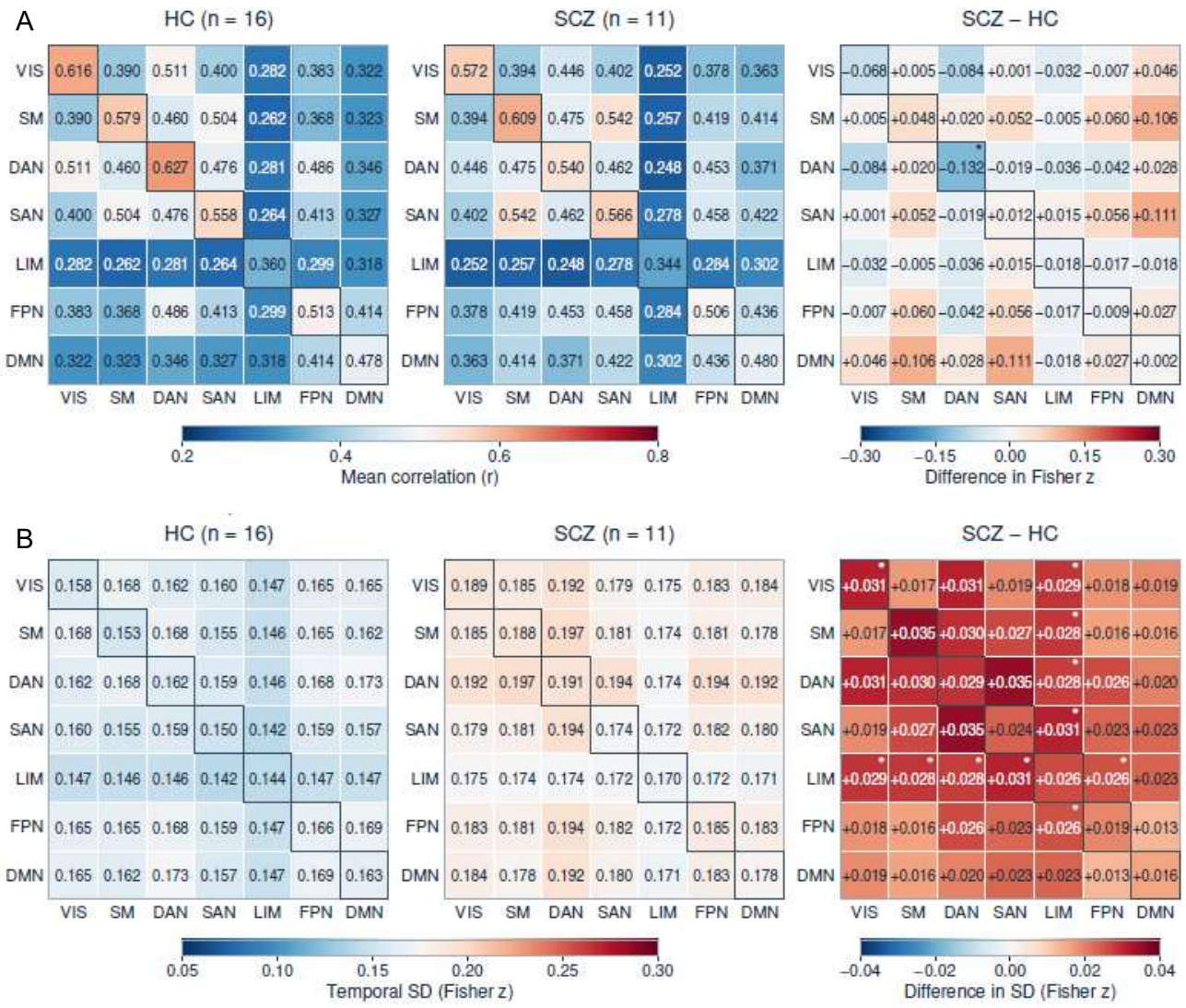


Figure 1. A. Static functional-connectivity matrices for HC (left), SCZ (centre), and the SCZ−HC difference (right). Group values represent inverse-transformed mean Fisher-z correlations; differences are expressed in Fisher-z units. B. Sliding-window connectivity variability for HC (left), SCZ (centre), and the SCZ−HC difference (right). Values represent the temporal standard deviation (SD) of Fisher-z correlations per connection, averaged within network blocks and groups. Matrices show the Visual, somatomotor (SM), attentional (DAN), salience (SAN), limbic (LIM), frontoparietal (FPN), and default mode (DMN) networks. Outlined diagonal cells indicate within-network estimates, excluding self-correlations. Positive differences are shown in red and negative differences in blue. * p<0.05.

2.2. Ignition and metastability

None of the five measures differed significantly between HC and SCZ (Fig. 2). Mean global synchronisation was lower in SCZ (mean Kuramoto order parameter, KOP: HC, 0.6056; SCZ, 0.5762; p>0.05), Fig 2A, as was intrinsic ignition (HC, 0.7796; SCZ, 0.7646; p>0.05), Fig 2B. Synchrony variability (STD-KOP: HC, 0.2030; SCZ, 0.1946; p>0.05) ; Fig 2C and ignition variability (STD-IGNITE: HC, 0.0623; SCZ, 0.0609; p>0.05), ; Fig 2D also showed no significant differences. VAR_{ev} was descriptively higher in SCZ but did not differ significantly between groups (HC, 0.004470; SCZ, 0.004886; p>0.05), Fig. 2E.

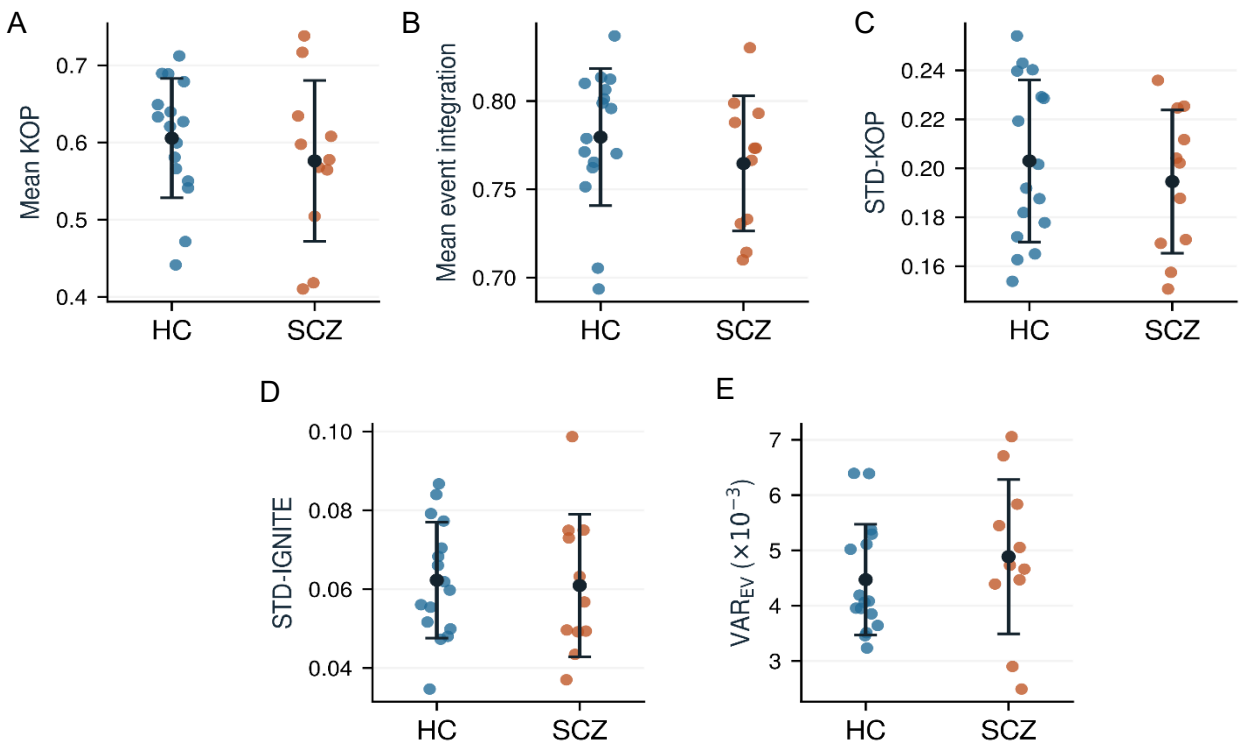


Figure 2. Intrinsic ignition and metastability. A. Mean Kuramoto order parameter (KOP), reflecting average global phase synchronisation. B. Mean intrinsic ignition, reflecting event-associated whole-brain integration. C. Temporal SD of KOP (STD-KOP). D. SD of event-associated integration within each region, averaged across regions (STD-IGNITE). E. Temporal variance of leading-eigenvector coefficients, averaged within and across five modes (VAR_{ev}). All measures were derived from AAL116 signals. Coloured points represent individual participants (HC; SCZ); black markers and bars indicate group mean ± SD.

The absence of a significant difference is consistent with previous work reporting no significant difference in global metastability between patients with schizophrenia and controls [10]. The same occur for VAR_{ev}, the nonsignificant group comparison can be considered alongside Hancock et al.'s findings, in which global VAR differences depended on the dataset and acquisition, with significant group by run interactions and no significant group difference in some runs [7].

2.3. Spatial Trapping Index (STI)

The Spatial Trapping Index (STI) quantified the effective number of modes across which each network relative spatial composition was distributed, with higher values indicating less selective representation. STI was higher in SCZ across all seven networks (Fig. 3A; Table 1). The largest increase occurred in the DMN; from 2.127 in HC to 3.482 in SCZ (SCZ−HC; Δ=1.356). FPN and limbic STI increased by 0.653 and 0.611, respectively, while the DAN had the highest absolute STI in SCZ (3.792). Smaller increases were observed in the SM (0.444), visual (0.146) and SAN (0.053) networks. Based on statistics analysis, the DMN difference provided a two-sided p = 0.0128 and remained significant after Holm correction across the two focal outcomes, STI and CAP (adjusted p = 0.0256). However, no network reached significance after the separate Holm correction across all seven STI comparisons; the adjusted p-value was 0.0896 (Table 1).

The observed positive DMN difference was retained in 8,958 of 9,999 within group participant bootstrap resamples (89.6%), with both group repertoires refitted in every replicate. The percentile 95% confidence interval for the SCZ−HC difference included zero (−0.378 to 1.563). Using these same bootstrap contrasts, an additional post hoc BCa analysis provided a 95% confidence interval of 1.139–2.221. The

BCa upper endpoint was effectively determined by the largest bootstrap contrast, indicating sensitivity at the distribution's extreme.

The DMN composition profiles illustrate the spatial pattern underlying its higher STI in SCZ (Fig. 3B). Mean DMN composition across the four analysed modes was descriptively similar between groups (HC, 24.36%; SCZ, 25.11%), but its distribution differed. In HC, DMN representation was concentrated in M2, accounting for 63.20%, 4.22%, 13.91% and 16.12% of the selected components in M2–M5, respectively. In SCZ, the corresponding proportions were 29.11%, 26.32%, 9.39% and 35.63%, indicating a more even distribution across modes. Thus, the higher STI reflected reduced spatial selectivity across configurations despite similar average composition.

Network	HC	SCZ	Difference (SCZ-HC)	P-value	Holm-adjusted P-value
Default mode network (DMN)	2.127	3.482	+1.356	0.0128	0.0896
Fronto-parietal network (FPN)	2.573	3.226	+0.653	0.1038	0.6228
Limbic network	2.704	3.315	+0.611	0.4028	1.0000
Dorsal attentional network (DAN)	3.223	3.792	+0.569	0.3928	1.0000
Somatomotor network (SM)	1.656	2.100	+0.444	0.2910	1.0000
Visual network	1.378	1.524	+0.146	0.8896	1.0000
Salience/ventral attentional network (SAN)	2.101	2.155	+0.053	0.9656	1.0000

Table 1. Spatial Trapping Index across seven functional networks. Values represent group STI estimates derived from the four selected modes (M2-M5). Differences are SCZ−HC and were calculated before rounding. Two-sided p-values were obtained from 9,999 participant-label permutations with group-specific repertoire estimation. The Holm-adjusted column corrects across all seven network comparisons; it is distinct from the two-comparison focal adjustment for DMN STI and CAP.

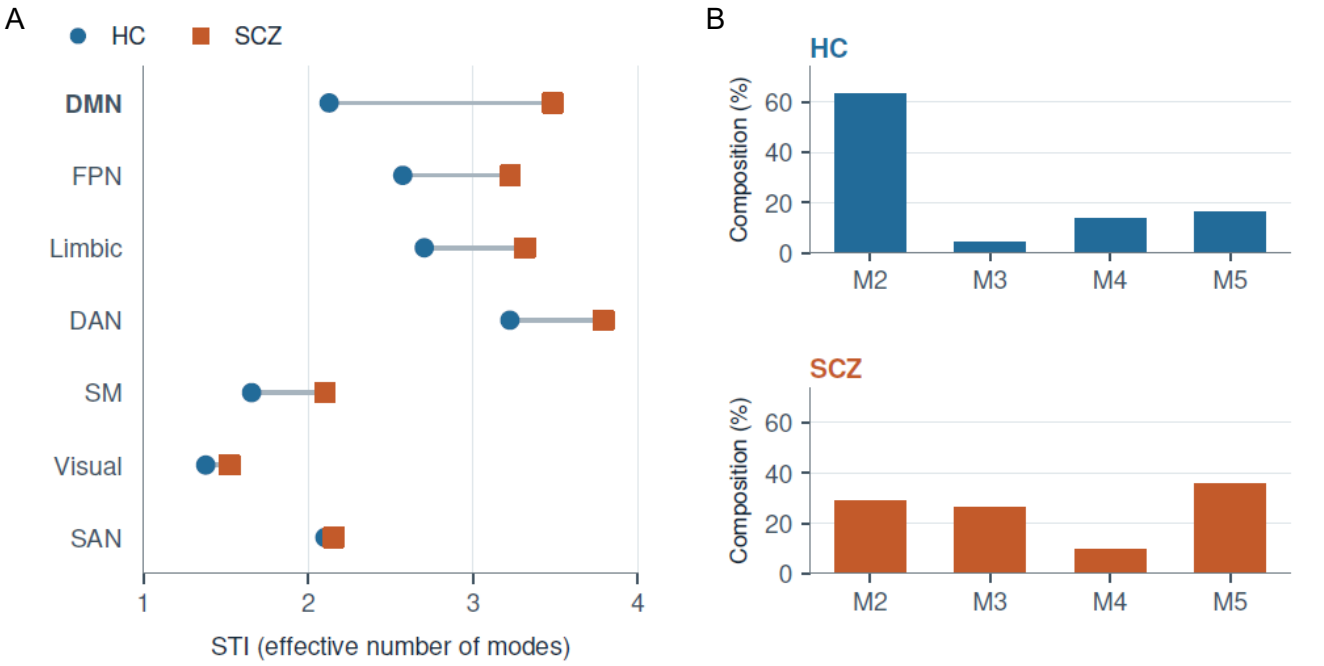


Figure 3. Spatial Trapping Index and DMN composition across recurrent modes. A, STI estimates for the seven networks in HC (blue circles) and SCZ (orange squares), ordered by decreasing SCZ−HC difference. Each marker represents a group-repertoire estimate. B, DMN composition within the selected components of M2–M5 in HC (top) and SCZ (bottom), expressed as the percentage of seven-network voxels assigned to the DMN. M1 was excluded because it represented a global phase alignment configuration. Higher STI indicates more evenly distributed network composition across modes. Mode labels are group-specific. HC, healthy controls; SCZ, schizophrenia.

2.4. Anterior–posterior co-participation (CAP)

We used CAP to assess whether selected medial anterior and posterior regions participated jointly in the same mode, complementing the network composition measured by STI. CAP decreased from 1.000 in

HC to 0.167 in SCZ (SCZ−HC Δ=−0.833; Fig. 4). Based on statistical analyses, the two-sided p-value was 0.0368 and remained $p < 0.05$ after Holm correction across the two focal outcomes, STI and CAP (adjusted $p = 0.0368$).

In HC, all six anterior and both posterior regions belonged to the selected component of M2, showing identical mode for all 12 anterior–posterior pairs. In SCZ, left medial orbitofrontal cortex and bilateral posterior cingulate cortex shared M5, accounting for the two pairs with Dice similarity equal to one. Right superior medial frontal, right medial orbitofrontal and right anterior cingulate regions belonged to M3, producing six pairs with disjoint anterior and posterior. Left superior medial frontal and left anterior cingulate regions had no shown in the selected components, accounting for the remaining four pairs (Table 2). Thus, lower CAP reflected both separation between anterior and posterior mode and absence of selected modes in two anterior regions. The pair counts describe anatomical relationships within each group series.

The observed negative difference was retained in 9,190 of 9,999 within group participant bootstrap resamples with repertoire refitting (91.9%). The percentile 95% confidence interval included zero (−1.000 to 0.167). An additional post hoc BCa analysis using the same bootstrap contrasts showed a 95% confidence interval of −1.000 to −0.611. Its lower endpoint coincided with the mathematical lower bound of the contrast, at which 311 bootstrap replicates accumulated.

AAL region	Anatomical Set	HC modes	SCZ modes
Superior medial frontal left	Anterior	M2	None
Superior medial frontal right	Anterior	M2	M3
Medial orbitofrontal left	Anterior	M2	M5
Medial orbitofrontal right	Anterior	M2	M3
Anterior cingulate left	Anterior	M2	None
Anterior cingulate right	Anterior	M2	M3
Posterior cingulate left	Posterior	M2	M5
Posterior cingulate right	Posterior	M2	M5

Table 2. Anatomical regions and modes used to calculate anterior–posterior co-participation. The anterior set comprised bilateral superior medial frontal, medial orbitofrontal and anterior cingulate regions; the posterior set comprised bilateral posterior cingulate regions. “None” indicates no selected mode across M2–M5.

A

AAL116 region	HC	SCZ
Superior medial frontal L	M2	—
Superior medial frontal R	M2	M3
Medial orbitofrontal L	M2	M5
Medial orbitofrontal R	M2	M3
Anterior cingulate L	M2	—
Anterior cingulate R	M2	M3
Posterior cingulate L	M2	M5
Posterior cingulate R	M2	M5

B

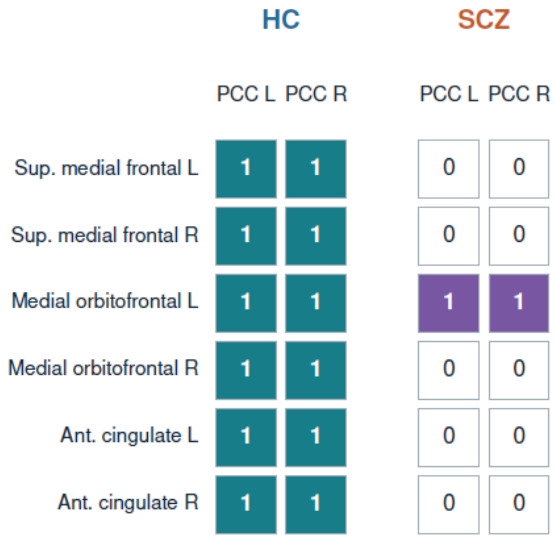


Figure 4. Anterior–posterior modal co-participation. A, Six medial anterior and two posterior cingulate regions in the selected modes for HC and SCZ. Coloured circles identify modes; dashes indicate no selected mode across M2–M5. B, Dice overlap for the 12 anterior–posterior anatomical pairs. All pairs shared mode in HC, whereas only the left medial orbitofrontal region shared mode with both posterior cingulate regions in SCZ. CAP, the mean pairwise overlap, was 1.000 in HC and 0.167 in SCZ (Δ= −0.833; two-sided permutation p = 0.0368; Holm-adjusted p = 0.0368 across the two focal outcomes). L, left; R, right; PCC, posterior cingulate cortex.

2.5. Anatomical distribution of anterior–posterior modal

To place the mode findings in their anatomical context, the modes underlying CAP were mapped onto medial views of both hemispheres (Fig. 5). The eight parcels were displayed over a standard anatomical template (MNI) and coloured according to their modes in the selected components of the modes M2–M5. In HC, all six anterior and both posterior regions shared M2 (blue). In SCZ, right superior medial frontal, right medial orbitofrontal and right anterior cingulate regions belonged to M3 (orange), whereas left medial orbitofrontal cortex and bilateral posterior cingulate cortex shared M5 (violet). Left superior medial frontal and left anterior cingulate regions had no mode in the selected components and were therefore uncoloured, although both remained represented in the model. Considered alongside the higher DMN STI, the findings show that a less selective distribution of DMN composition across modes coexisted with reduced joint modal participation of the selected medial anterior and posterior regions.

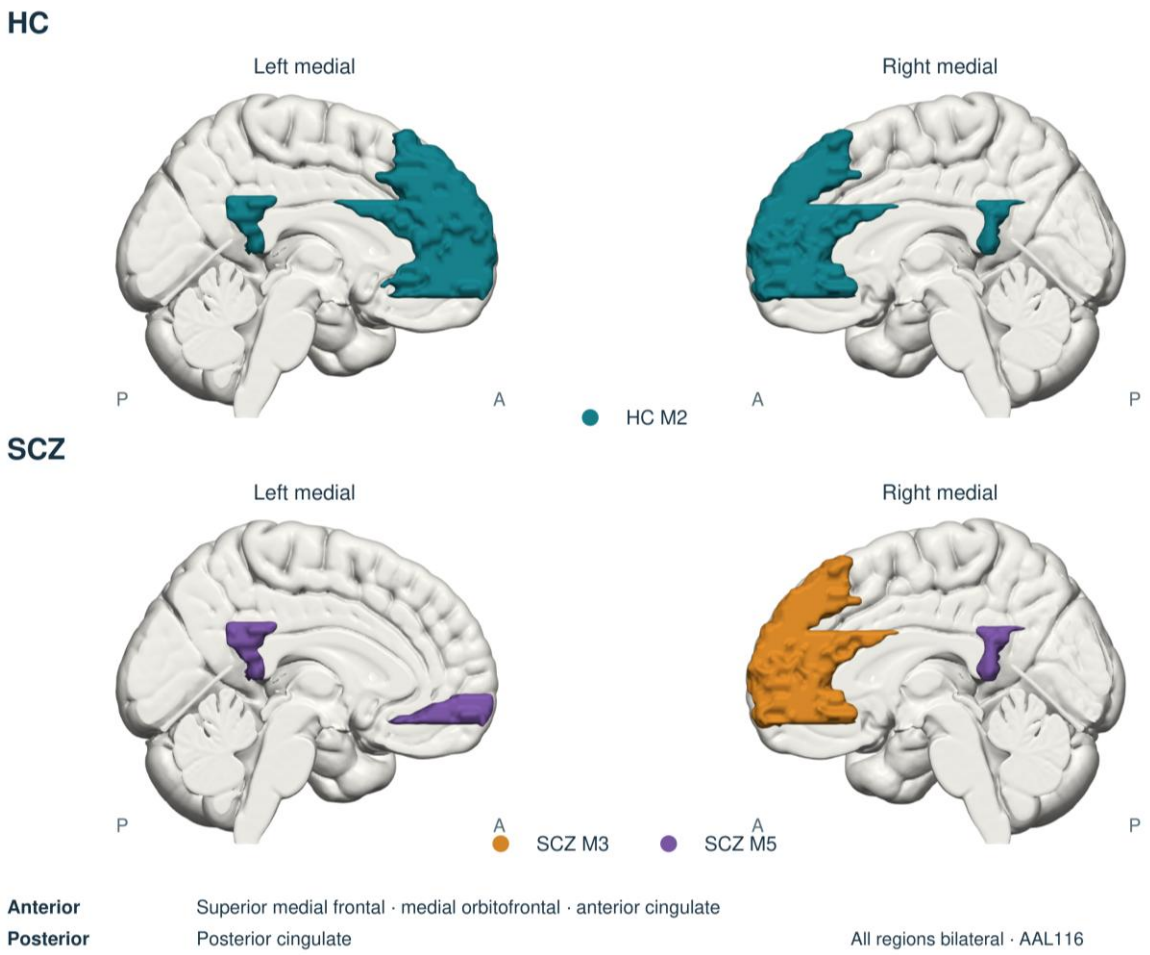


Figure 5. Anatomical distribution of anterior–posterior modal. Medial views of the left and right hemispheres show the selected AAL116 regions in HC (top) and SCZ (bottom). In HC, all eight regions shared M2 (blue). In SCZ, the right superior medial frontal, medial orbitofrontal and anterior cingulate regions belonged to M3 (orange), while the left medial orbitofrontal and bilateral posterior cingulate regions shared M5 (purple). The left superior medial frontal and anterior cingulate regions had no selected mode and remain uncoloured. Colours indicate mode, not activation. Shared anterior–posterior pairs numbered 12/12 in HC and 2/12 in SCZ. A, anterior; P, posterior.

3. Discussion

Static and dynamic connectivity revealed complementary aspects of functional organisation in this cohort. In SCZ, static connectivity was lower within the DAN, whereas within-DMN connectivity was descriptively similar between groups. This pattern is consistent with previous evidence of reduced dorsal attention connectivity and differential involvement of resting-state networks in schizophrenia [11]. Alongside these static findings, dynamic connectivity variability was descriptively higher across network blocks, with differences predominantly involving the limbic network. Increased temporal variability has also been reported in visual and related temporal regions in schizophrenia [19], providing a support for altered connectivity fluctuations, although the anatomical patterns and analytical approaches differed. Together, these observations suggest that average connectivity and its variation over time provide distinct information about network organisation.

These differences were not accompanied by significant changes in global synchronisation, intrinsic ignition, STD-KOP, STD-IGNITE or leading-eigenvector variance. The STD-KOP result is consistent with previous work reporting reduced global synchrony without a significant difference in global metastability [10]. Other study has shown that phase-locking variability differs across datasets and acquisitions,

including interactions between diagnostic group and run [7]. These studies shown that abnormalities in functional connectivity need not be accompanied by a consistent difference in every global measure of collective dynamics. The relationship between connectivity and global dynamics therefore depends partly on the property being measured: fluctuations in correlations need not be accompanied by corresponding changes in whole-brain phase synchronisation or event-associated integration. These measures also leave open the question of how regional contributions are organised within the collective patterns.

Examining this spatial organisation can help place the findings in context. Global measurements do not fully specify the anatomical arrangement of activity, and network averages can obscure differences in regional participation. Similar results may therefore accompany different configurations. Following networks across recurrent modes, and identifying which regions participate together, provides additional information about these spatial relationships.

From this perspective, the DMN showed a more profile in SCZ despite a descriptively similar mean contribution across modes. In HC, the DMN accounted for 63.2% of one selected mode component and substantially smaller proportions of the others. In SCZ, its contribution was distributed more evenly across the four analysed modes. Considering that recurrent phase configurations can correspond predominantly to recognisable functional networks [6], our analysis extends this perspective by following the representation of a given network, rather than characterising each configuration only by its predominant network. The higher STI (DMN) therefore reflected reduced selectivity of its spatial representation, a difference that was not apparent from its average composition. Also, this distinction between average composition and mode selectivity provides a complementary perspective on previous temporal findings. Kottaram et al.,[14] reported lower occupancy but longer visits to a mode characterised by high DMN and low sensory activity, while Farinha et al.[20] found a lower probability of remaining in a DMN-related LEiDA modes in schizophrenia. Leaving a DMN-dominant configuration does not necessarily mean entering one without DMN involvement. Reduced occupancy of a particular state could coexist with DMN representation spread across several configurations. This relationship remains to be tested within the same dataset, because STI does not incorporate occupancy, dwell time or transition probabilities. Spatial trapping therefore describes how selectively a network is represented across modes. This focus on representation also raises a complementary question: whether the spatial pattern of each individual state remains consistent. Wang et al., reported reduced engagement of a visual–salience co-activation mode despite broadly conserved spatial patterns across the psychosis continuum [21]. Such findings are compatible with the possibility that recognisable modes persist while their recruitment or network composition differs. STI addresses the distribution of a fixed network annotation across configurations, rather than the reproducibility of an individual mode map. These properties should be investigated separately, particularly because amplitude-based co-activation modes and phase-based modes capture different features of the BOLD signal.

The lower CAP adds anatomical detail to the broader distribution of DMN representation. In HC, all eight sampled medial anterior and posterior regions shared a selected component. In SCZ, three right anterior regions participated in a different mode from the posterior cingulate regions, while two left anterior regions had no selected. Shared participation remained between the left medial orbitofrontal cortex and bilateral posterior cingulate cortex. Thus, the observed pattern represented partial separation of anterior and posterior mode. A network can be represented across several configurations while its constituent regions participate less consistently together; higher STI and lower CAP describe these complementary aspects of spatial organisation. This is consistent with evidence that schizophrenia affects relationships within the DMN unevenly. Previous works have shown a diminished interaction among DMN subsystems [12], as well as abnormalities involving anterior and posterior regions whose expression varied across connectivity states [13] . CAP contributes a different description of this organisation by measuring shared membership in selected mode components. Its reduction does not directly demonstrate weaker physiological coupling:

regions without selected membership remain part of the whole-brain configuration, and their participation on the complementary side of the centroid is not included in the index.

The functional relevance of these medial territories provides a rationale for future cognitive investigations. Andrews-Hanna et al. [15] associated anterior medial prefrontal and posterior cingulate regions with personally significant and affective self-referential processing. Holt et al. [22] subsequently reported an anterior-to-posterior shift in midline activity during self-reflection in schizophrenia, together with altered resting connectivity. Based on these observations, we motivated to test whether the spatial organisation identified here relates to self-referential processing, source attribution or reality monitoring. However, our results do not establish such relationships, because STI and CAP describe group repertoires and were not linked to performance on these tasks.

A possible account concerns the regulation of interactions through which distributed regions form coordinated configurations. The disconnection framework [2] emphasises abnormal modulation of synaptic efficacy and its consequences for functional integration. Within this framework, altered regulation of interactions could affect how selectively DMN regions assemble across configurations. Although the present spatial measures do not directly identify the underlying mechanisms, computational modelling offers a way to explore how these patterns might arise. Previous work showed that reduced global coupling or increased background noise could reproduce aspects of the connectivity and synchrony abnormalities observed in schizophrenia [10]. Extending these models to examine whether they also reproduce higher STI and lower CAP could help clarify how altered interactions shape the spatial organisation. In particular, these measures could help distinguish models that yield similar global dynamics but differ in how DMN regions participate across modes.

Understanding the significance of these patterns also requires relating them to the experiences and difficulties encountered by people with schizophrenia. Social functioning is particularly relevant because previous studies have linked DMN connectivity to perceived isolation and loneliness. Spreng et al., [23] associated perceived social isolation with stronger within-DMN connectivity, whereas Saris et al., [24] linked social dysfunction and loneliness to reduced prefrontal DMN connectivity across diagnostic groups. These differing findings suggest that the relationship depends on both the population and the aspect of network organisation examined. Assessing modal selectivity and anterior–posterior co-participation alongside loneliness and social participation could help establish whether the spatial properties identified here have relevance to everyday functioning.

Establishing these relationships would provide a basis for investigating whether changes in DMN organisation accompany meaningful clinical improvement. Cognitive training in schizophrenia could improve reality monitoring and increase medial prefrontal recruitment [25], suggesting that processes relevant to the present interpretation may be modifiable. Longitudinal and intervention studies could therefore examine whether changes in mode selectivity and anterior–posterior co-participation accompany improvements in self-related cognition and social functioning. Following independent replication and validation at the individual level, STI and CAP could provide complementary research outcomes for determining which aspects of distributed network organisation are responsive to intervention and relevant to recovery in schizophrenia.

Several methodological and clinical factors should be considered when interpreting these findings. Although the sensitivity analyses supported their consistency within this cohort, some clarifications should be detailed.

The spatial findings should be interpreted in relation to the choices used to define the modal repertoires. The five-mode solution provided a common resolution for comparing groups, with four modes contributing to STI and CAP after exclusion of the global mode, M1. Although this choice has precedents in LEiDA research, it does not establish an optimal repertoire size. The selected components also depend on the

eigenvector orientation convention. Orienting vectors and centroids to have a non-negative regional sum provided a consistent rule for selecting one pole; coefficient signs do not indicate activation or deactivation. CAP consequently describes shared membership within that selected pole and among a restricted set of medial frontal, anterior cingulate and posterior cingulate parcels, rather than all anterior–posterior relationships within the DMN.

The higher DMN STI support its consistency across the spatial definitions examined. Both focal contrasts also retained their direction in all participant-omission refits and balanced HC subsets, and in 89.6% and 91.9% of bootstrap resamples for STI and CAP, respectively. These checks address sensitivity within the observed sample. Percentile confidence intervals included zero, whereas the post hoc BCa intervals excluded zero but had extreme endpoints. Permutation testing therefore remained the primary inferential analysis.

The small sample size and short resting-state acquisition can be a limitation. In addition, the cross-sectional design and medication exposure prevent the observed differences from being attributed specifically to illness mechanisms.

Conclusion

Here, we show that schizophrenia was associated with more evenly distributed DMN representation across recurrent brain modes and reduced co-participation of selected anterior and posterior regions. STI and CAP captured complementary aspects of this spatial organisation, whose clinical relevance requires independent validation.

4. Materials and methods

4.1. Participants

The participants were recruited from local announcements in Tenerife (Spain) and comprised 27 participants: 16 healthy controls (HC) and 11 participants with schizophrenia (SCZ). Mean ages were 38.9 ±10.3 years in HC and 45± 11.8 years in SCZ. Participant demography are summarised in Table 3.

Participants in the SCZ group met the following clinical criteria: (i) a diagnosis of schizophrenia according to DSM-5-TR criteria [26] ; (ii) a diagnosis established more than five years before MRI acquisition; (iii) no acute psychotic exacerbation at the time of scanning or during the preceding 12 months; (iv) global cognitive status using the 35-point Mini-Examen Cognoscitive (MEC-35) [27] .

Diagnostic eligibility and clinical status were verified by a psychiatrist (P.B.) through review of clinical assessments documented around MRI acquisition and longitudinal psychiatric records. HC reported no psychiatric or neurological disorder.

Exclusion criteria for both groups included a history of head trauma, substance abuse during the preceding six months and contraindications to MRI.

Patient (SCZ)	Gender	Age	Education	Marital status	Medication	MEC 35
SCZ1	M	22	Elementary	Single	Atypical Antipsychotic + Sedative	33
SCZ2	M	47	Middle school	Single	Typical Antipsychotic + SSRI	35
SCZ3	F	47	Elementary	Single	Atypical Antipsychotic + Mood stabilizer	30
SCZ4	M	64	Bachelor	Single	Atypical Antipsychotic + SSRI	30
SCZ5	F	36	Elementary	Single	Atypical Antipsychotic (LAI) + Sedative	30
SCZ6	F	32	Bachelor	Single	Atypical Antipsychotic (LAI)	35
SCZ7	M	52	Bachelor	Married	Atypical Antipsychotic (LAI) + Mood stabilizer	34
SCZ8	M	57	Elementary	Single	Atypical Antipsychotic (LAI)	24
SCZ9	M	41	High school	Single	Atypical Antipsychotic (LAI)	33
SCZ10	F	51	Elementary	Single	Typical Antipsychotic + Mood stabilizer + Sedative	26
SCZ11	M	46	Elementary	Single	Atypical Antipsychotic (LAI) + Mood stabilizer + Sedative	31

Table 3. Demography of participants with schizophrenia. The table summarises gender, age, MEC-35 scores (Mini-Examen Cognoscitivo-35) and recorded medications for the 11 participants with schizophrenia. SCZ, schizophrenia; MEC-35, 35-point Mini-Examen cognoscitive; M, male; F, female; SCZ, schizophrenia; LAI, long-acting injectable. Typical: first-generation antipsychotic; Atypical: second-generation antipsychotic. LAI antipsychotics correspond to paliperidone palmitate formulations. MEC-35 scores range from 0 to 35; higher scores indicating better cognitive performance (group mean ± SD, 31.0 ± 3.5; observed range, 24–35).

4.2. Ethical approval and consent to participate

This study was conducted in Hospital Universitario Nuestra Señora de Candelaria (Tenerife, Spain), followed the Strengthening the Reporting of Observational Studies in Epidemiology (STROBE) recommendations [28]

The study was conducted in accordance with the Declaration of Helsinki and it was approved by the Ethics Committee of Hospital Universitario Nuestra Señora de Candelaria (CHUNSC_2026_33), Tenerife, Spain.

In participants with schizophrenia, capacity to provide informed consent was assessed jointly by two co-authors, the neuropsychologist (N.C.E.) and the psychiatrist (P.B.), using a clinical interview and the MacArthur Competence Assessment Tool for Clinical Research (MacCAT-CR). The assessment addressed understanding of the study information, appreciation of its personal implications, reasoning about participation, and the ability to express a choice. The findings informed the joint clinical judgement regarding each participant's capacity to consent. Nine of the 11 participants with schizophrenia were assessed as able to provide their own informed consent and signed the consent form themselves. The remaining two participants were judged unable to provide independent informed consent for this study.

For these participants, written informed consent was obtained from their legally authorised representatives, with the consent procedure coordinated through the Instituto Insular de Atención Social y Sociosanitaria (IASS), Tenerife. All 16 healthy controls provided their own written informed consent.

4.3. MRI acquisition

MRI data were acquired using a 3-T MAGNETOM Prisma scanner (Siemens Healthineers) equipped with a 64-channel head coil. During resting-state functional imaging, participants were instructed to keep their eyes open and fixate on a cross. Functional images were acquired in a single continuous run using a T2*-weighted gradient-echo echo-planar imaging sequence (TR, 1.5 s; TE, 33 ms; flip angle, 72°; 72 axial slices; slice thickness, 2.5 mm without a gap; field of view, approximately 250 mm). Each analysed run comprised 120 volumes, corresponding to 180 s. High-resolution T1-weighted structural images were acquired with a TR of 2.30 s, a TE of 2.32 ms, a flip angle of 8°, a matrix of 256 × 256, an in-plane resolution of 0.98 × 0.98 mm, and a slice thickness of 0.9 mm.

4.4. Data analysis

Data pre-processing was performed using SPM25 in MATLAB (R2026a). Functional images were realigned, co-registered to each participant's T1-weighted structural image, and normalised to Montreal Neurological Institute (MNI) space using unified segmentation [29]. Images were resampled to 2-mm isotropic voxels and smoothed with an 8-mm full-width-at-half-maximum Gaussian kernel.

A common temporal pre-processing pipeline was applied to the regional time series used in all analyses. Each region-of-interest (ROI) time series was first linearly detrended. Nuisance regression was subsequently performed using the whole-brain global signal, mean white matter (WM) and cerebrospinal fluid (CSF) signals, and a 24-parameter head-motion model comprising the six realignment parameters, their first temporal derivatives, and the squared terms of both sets. The resulting time series were band-pass filtered at 0.01–0.1 Hz using a zero-phase Butterworth filter with identical specifications across analyses. For those phase-analyses, the instantaneous phase of each filtered time series was extracted using the Hilbert transform.

Analyses combined the AAL116 anatomical parcellation [30] with the Yeo seven-network framework [31] AAL116 provided the cortical, subcortical and cerebellar signals used for LEiDA and global measures, together with the anatomical regions used to define modal components and anterior–posterior co-

participation, and characterised the spatial composition of modal components through voxel-wise overlap with AAL116 for STI calculation.

4.5. Functional connectivity

Static and dynamic connectivity were assessed within and between the seven Yeo functional networks [31]: visual (VIS), somatomotor (SM), dorsal attention (DAN), salience/ventral attention (SAN), limbic (LIM), frontoparietal control (FPN), and default mode (DMN). For each participant, static connectivity was calculated using Pearson correlations between pre-processed voxel-level BOLD signals. Correlations were Fisher-transformed and averaged within each network and between networks, excluding self-correlations.

Dynamic connectivity was assessed using 60s sliding windows advanced in 1.5s steps. Pearson correlations were calculated within each window and Fisher-transformed. For each connection, the temporal standard deviation of its Fisher z values was then calculated across windows. Thus, this measure represents the average variability of individual connections.

4.6. Phase configurations and recurrent modes

Leading Eigenvector Dynamics Analysis (LEiDA) was used to identify recurrent whole-brain configurations of BOLD phase alignment from the pre-processed AAL116 regional signals [5] [30]. This generated an instantaneous symmetric phase-locking matrix for each time point. The unit leading eigenvector, corresponding to the largest eigenvalue, was retained as a representation of the dominant whole-brain phase-locking configuration [5][6]. Each of its 116 coefficients represented the loading of one anatomical region on this dominant spatial pattern. Coefficients of the same sign identified the same pole of the pattern, whereas opposite signs distinguished its two poles. Before clustering, the algebraic sign ambiguity was resolved by multiplying each eigenvector by −1 whenever the sum of its regional coefficients was negative. The complete oriented eigenvectors, retaining both positive and negative coefficients, were pooled across retained time points and participants within each group. Separate HC and SCZ series were then estimated using spherical k-means with cosine distance and $\boldsymbol{k = 5}$ [7]. Clustering was performed with 300 initialisations per group, and the solution with the lowest mean within-cluster cosine distance was retained. Each time point was assigned to the centroid with the greatest cosine similarity. The resulting centroids were also oriented to have a non-negative sum of regional coefficients.

For spatial characterisation, centroids were also oriented to have non-negative coefficient sums. M1 was identified as the mode with the smallest proportion of negative coefficients and had coefficients of the same sign across all 116 regions in both observed groups. The remaining modes were as known as M2–M5 were ordered by decreasing fractional occupancy within each group. M1 was excluded from the subsequent STI and CAP analysis. For each mode, the selected component comprised regions with negative centroid coefficients, and regions with coefficients equal to zero were not included in this selected component [6] [20].

4.7. Global synchronisation, ignition and signatures of metastability

Global measures were calculated from the pre-processed BOLD signals of the AAL116 regions and their instantaneous phases, obtained as described above. Global phase synchronisation was quantified using the Kuramoto order parameter (KOP), which measures the alignment of regional phases at each time point, with values approaching 1 indicating greater synchronisation [32]. Its temporal mean provided the measure of average global synchronisation, whereas its sample temporal standard deviation (STD-KOP) quantified fluctuations in global synchronisation and was used as a signature of metastability [7] [33].

Intrinsic ignition measured the whole-brain integration associated with regional BOLD events [9]. Events were identified as upward crossings of a threshold of 1 standard deviation in each region's z-scored BOLD signal. At each time point, phase similarity between regions was calculated as e^{-3d}, where d is their circular phase distance in radians. Integration was defined as the proportion of regions belonging to the largest connected component, averaged across thresholds. For each event, integration was averaged over four consecutive samples, beginning at event onset; incomplete event windows were excluded. Event-associated integration was first averaged within each region and then equally across regions to obtain mean intrinsic ignition.

Ignition variability (STD-IGNITE) captured how consistently events within a region were associated with whole-brain integration [34]. For each region with at least two complete event windows, the standard deviation of event-associated integration was calculated. These regional standard deviations were then averaged with equal weight to obtain a participant level estimate. Higher values therefore indicate greater variability in integration across events within regions, rather than greater differences in mean ignition between regions.

Following the community-based approach to metastability proposed by Hancock et al.,[7] we calculated variance measure (VAR_{ev}) using the oriented leading eigenvectors and modes defined above (LEiDA analysis). For each participant, the population temporal variance of each regional eigenvector coefficient was calculated across all retained time points, irrespective of the mode assigned to each time point. Regional variances were averaged within each of five mode communities and subsequently averaged with equal weight across communities. The global mode (M1) included all 116 regions, whereas the four modes comprised the selected regional components of their respective centroids and could overlap.

This measure quantified temporal changes in regional contributions to the dominant phase alignment pattern. STD-KOP, STD-IGNITE and VAR_{ev} were interpreted as complementary signatures of metastability, reflecting fluctuations in global synchronisation, event associated integration and regional phase alignment, respectively [7].

4.8. Network composition and Spatial Trapping Index (STI)

The Spatial Trapping Index (STI) quantifies the effective number of modes across which a network's relative spatial representation is distributed. STI was calculated using only the four modes (M2–M5). The global mode (M1) had centroid coefficients of the same sign across all 116 AAL regions in both groups, representing a whole-brain phase-alignment configuration. It was therefore excluded to focus the index on network representation within the differentiated components of the modes.

Network composition was assessed separately for the HC and SCZ series by combining the AAL116 parcellation with the seven-network atlas. AAL116 defined the regions used to extract BOLD signals and identify modes, while seven-network atlas provided the cortical network labels. Seven-network atlas labels were first resampled onto the AAL grid using the atlases' spatial transformations and nearest-neighbour interpolation. For each AAL region, we then counted the voxels belonging to each seven-network network, allowing a single region to contribute to more than one network. These overlap counts were summed across the AAL regions included in each selected modal component to determine its network composition.

For each AAL region r , we counted the voxels assigned to each seven-network n, defining the atlas-overlap weights W_{rn}. These weights were fixed across modes and groups. Each mode m selected a subset of AAL regions: $S_{mr} = 1$; if region r had a negative coefficient in that mode's-oriented centroid, and $S_{mr} = 0$ otherwise. The number of voxels assigned to network n within the selected component of mode m was therefore:

$$A_{mn} = \sum_{r=1}^{116} S_{mr} W_{rn} \quad (1)$$

Its relative network composition was calculated as:

$$C_{mn} = \frac{A_{mn}}{\sum_{l=1}^{7} A_{ml}} \quad (2)$$

where the denominator is the total number of voxels assigned to any of the seven-networks l within that selected mode component.

For each network n, the composition values from the four modes were normalised to sum to one:

$$q_{mn} = \frac{C_{mn}}{C_{2n}+C_{3n}+C_{4n}+C_{5n}} \qquad m \in \{2,3,4,5\} \quad (3)$$

where q_{mn} denotes the contribution of mode m to the network's composition profile across the four modes. The Spatial Trapping Index was then calculated as:

$$STI_n = \frac{1}{q_{2n}^2+q_{3n}^2+q_{4n}^2+q_{5n}^2} \quad (4)$$

This corresponds to Hill's effective diversity of order two [17], with modes treated as categories and their normalised composition values as weights. STI ranges from 1, when the network is represented in only one selected mode component, to 4, when its composition is equal across all four mode components. Higher values therefore indicate less selective representation across modes. STI was left undefined when the network had zero composition in every mode.

4.9. Anterior–posterior mode co-participation (CAP)

STI describes how a network's spatial composition is distributed across modes but does not establish whether its anterior and posterior regions participate in the same mode components. We therefore constructed the anterior–posterior mode co-participation index (CAP) to examine this relationship within a selected anatomical set.

The anterior set comprised bilateral superior medial frontal cortex, medial orbitofrontal cortex and anterior cingulate cortex. The posterior set comprised bilateral posterior cingulate cortex. These regions were selected to operationalise a restricted comparison between medial anterior territories and the posterior cingulate, motivated by the anatomical organisation of the DMN [15]. This eight-region selection constitutes a specific definition rather than a comprehensive anterior–posterior partition of the network.

Following the descriptors S_{mr} defined above, mode co-participation between an anterior region a and a posterior region p was calculated using Dice's coefficient [18]:

$$D_{ap} = \frac{2\sum_m S_{ma}S_{mp}}{\sum_m S_{ma} + \sum_m S_{mp}} \quad (5)$$

where the numerator counts twice the number of modes in which both regions belong to the selected component, while the denominator sums their individual mode. For each anterior–posterior pair, we counted the modes in which both regions belonged to the selected component. Dice's coefficient [18] was calculated as twice this shared count divided by the sum of the two regions' individual counts. A value of 1 indicates that both regions participate in exactly the same modes, whereas 0 indicates that they share none. Intermediate values indicate partial overlap. Pairs in which neither region participated in any selected component were excluded.

To summarise co-participation between the anterior and posterior sets, each of the six anterior regions was compared with both posterior regions. To comparison, 12 pairs were included within and across hemispheres. CAP was calculated as the equally weighted mean of the estimable Dice coefficients:

$$CAP = \frac{1}{N_{est}} \sum_{est} D_{ap} \quad (6)$$

where N_{est} is the number of estimable pairs; If only one region had no selected mode, the pair contributed zero. If neither region had a selected mode, the pair was undefined and excluded. CAP ranges from 0 to 1 whenever at least one pair is estimable. Higher values indicate more similar anterior and posterior mode. Lower values reflect participation in different selected mode components or the absence of selected mode for one region.

4.10. Statistical analysis

4.10.1. General framework

Statistical analyses were performed using MATLAB (R2026a; MathWorks, Natick, MA, USA) and Python (3.14.5; Python Software Foundation). Participants were the sampling units, and all between-group contrasts were expressed as SCZ minus HC. Tests were two-sided, with a significance threshold of α = 0.05 and correction for multiple comparisons. Each permutation analysis used 9,999 unique random reallocations of participant labels, preserving the group sizes and excluding the observed allocation and duplicate reallocations.

4.10.2. Static and dynamic connectivity

Static and dynamic connectivity were compared using Welch-studentised differences in participant estimates. Static group matrices displayed the inverse Fisher transform of the mean participant estimates; static difference matrices and inference used Fisher-z normalized units. Dynamic group matrices displayed mean participant variability, and differences were expressed in standard deviation; SD, (Fisher z) units. For static and dynamic connectivity, two-sided p-values were calculated from the proportion of absolute permuted Welch statistics at least as large as the absolute observed statistic, including numerical ties within 10^{-12}. A plus-one correction was applied to both the exceedance count and the number of permutations [35].

4.10.3. Global synchronisation, ignition and variability measures.

Global synchronisation, intrinsic ignition, STD-KOP, STD-IGNITE and VAR_{ev} were summarised as group means and standard deviations and compared using Welch-studentised mean differences. For VAR_{ev}, participant estimates were recalculated using the modes obtained from the group series refitted under each label allocation. The remaining global estimates were fixed participant quantities. Two-sided p-values used the inclusive equal-tail procedure defined in the Eq. 7, applied to the observed and permuted Welch statistics.

4.10.4. Group-derived spatial outcomes

DMN STI and CAP were the two focal outcomes. Each index was calculated from a group mode, and its test statistic was the difference between the SCZ and HC index values. For every participant-label allocation, both group modes were refitted using the clustering by LEiDA explained previously. This incorporated repertoire estimation into the permutation distribution under the assumption of participant-label exchangeability [36].

For these spatial contrasts, two-sided permutation p-values were calculated as twice the smaller inclusive tail probability, capped at 1:

$$p = min\left[1{,}2 \min\left(\frac{1+N_{\leq}}{B+1}, \frac{1+N_{\geq}}{B+1}\right)\right] \quad (7)$$

where $B = 9{,}999$, $N_{\leq}$ and $N_{\geq}$ count permuted contrasts at or below, and at or above, the observed contrast, respectively. Numerical ties were included using a tolerance of 10^{-15}. The plus-one correction accounted for Monte Carlo permutation sampling and prevented zero p-values [35].

Holm's step-down procedure [37] controlled the familywise error rate across the two focal tests, DMN STI and CAP. The seven-network STI survey was additionally reported with a separate Holm correction. The focal family was developed within this cohort and was not prospectively independent of the seven-network analysis. For connectivity, Holm-adjusted p-values were calculated across the 28 network blocks separately for each endpoint and processing variant. Additional adjustments covered 112 comparisons across both variants.

4.10.5. Bootstrap stability and confidence intervals.

Stability of the two focal contrasts for STI and CAP, was assessed using 9,999 bootstrap resamples drawn independently with replacement within each group. The resulting bootstrap distributions are illustrated in Supplementary Material Fig. 1, with STI in the upper panels and CAP in the lower panels. The left panels display the distributions of the refitted group estimates for HC and SCZ, whereas the right panels display the distributions of their corresponding SCZ−HC contrasts.

Directional consistency was calculated as the proportion of contrasts retaining the observed sign: ΔSTI*> 10^{-12} for DMN STI and ΔCAP*<10^{-12} for CAP, where the asterisk denotes a bootstrap estimate. Contrasts within 10^{-12} of zero remained in the denominator of 9,999, but were not counted as directionally consistent. Percentile 95% confidence intervals were obtained from the 2.5th and 97.5th percentiles of the bootstrap contrasts using linear interpolation. All numerical summaries were calculated directly from the individual bootstrap estimates; the smoothed density curves were used for visualisation.

Bias-corrected and accelerated (BCa), 95% confidence intervals were subsequently evaluated as a post hoc complementary analysis of the same 9,999 bootstrap contrasts [38]. For each outcome, let $\widehat{\Delta}$ denote the observed SCZ−HC contrast and Δ_b^* its estimate in bootstrap replicate b.

The bias-correction term was calculated as $z_o = \Phi^{-1}\left(\frac{N_{<}+\frac{1}{2}N_{=}}{B}\right)$, where $B = 9{,}999$, Φ^{-1} is the standard normal quantile function, $N_{<}$ counts bootstrap satisfying $\Delta_b^* < \widehat{\Delta} - 10^{-12}$, and $N_{=}$ counts ties satisfying $\left|\Delta_b^* - \widehat{\Delta}\right| \leq 10^{-12}$.

Acceleration was estimated using a participant-level jackknife, omitting each participant in turn and refitting the affected group's repertoire while retaining the other group's observed repertoire. Let $\widehat{\Delta_{g,(-\iota)}}$ denote the contrast after omitting participant i from group i, and let $\widehat{\Delta_{g,(-\cdot)}}$ denote the mean of the leave-one-out contrasts within that group. The weighted influence values were calculated as;

$u_{g,i} = \frac{n_g - 1}{n_g}\left(\widehat{\Delta_{g,(-\cdot)}} - \widehat{\Delta_{g,(-\iota)}}\right)$, where n_g denotes the group size. These values were combined across both groups to estimate acceleration $\hat{a} = \frac{\sum_g \sum_{i=1}^{n_g} u_{g,i}^3}{6\left(\sum_g \sum_{i=1}^{n_g} u_{g,i}^2\right)^{3/2}}$. For each quantile probability $p \in \{0.025, 0.075\}$, the adjusted BCa probability was: $pBC_a = \Phi\left[z_0 + \frac{z_0 + \Phi^{-1}(p)}{1 - \hat{a}[z_0 + \Phi^{-1}(p)]}\right]$, where Φ is the standard normal cumulative distribution function. The confidence interval endpoints were obtained from the bootstrap contrasts at these adjusted probabilities using linear interpolation

Data availability

Requests code and participant data, including regional time series and raw MRI data, should be directed to the corresponding author, Jesús Martín-Fernández (jesusmarfdez9@gmail.com). Access to participant

data is subject to participant consent, institutional authorisation and applicable ethical and data protection requirements.

Acknowledgements

We are grateful to all participants and their families for their time, trust and support of research into schizophrenia. Their contribution makes it possible to investigate the brain's dynamic organisation, with the long-term aim of deepening our understanding of the disorder and improving care for those living with it.

The corresponding author wishes to express his particular gratitude to his doctoral supervisor and co-author, F.P.R., for teaching him to approach mental illness through the lens of complex dynamical systems and to look beyond any single explanatory perspective. His mentorship has encouraged a way of thinking that seeks understanding in the relationships between different levels of brain organisation while remaining attentive to the experience of the individual.

Funding

This research received no specific grant funding.

Competing interests

The authors report no competing interests.

References

1. Friston, K. The dysconnection hypothesis of schizophrenia: a 30-year update. *World Psychiatry* **25**, 225–226 (2026).
2. Friston, K. J. The disconnection hypothesis. *Schizophr. Res.* **30**, 115–125 (1998).
3. Deco, G., Jirsa, V., McIntosh, A. R., Sporns, O. & Kötter, R. Key role of coupling, delay, and noise in resting brain fluctuations. *Proceedings of the National Academy of Sciences* **106**, 10302–10307 (2009).
4. Deco, G., Jirsa, V. K. & McIntosh, A. R. Emerging concepts for the dynamical organization of resting-state activity in the brain. *Nat. Rev. Neurosci.* **12**, 43–56 (2011).
5. Cabral, J. *et al.* Cognitive performance in healthy older adults relates to spontaneous switching between states of functional connectivity during rest. *Sci. Rep.* **7**, 5135 (2017).
6. Vohryzek, J., Deco, G., Cessac, B., Kringelbach, M. L. & Cabral, J. Ghost Attractors in Spontaneous Brain Activity: Recurrent Excursions Into Functionally-Relevant BOLD Phase-Locking States. *Front. Syst. Neurosci.* **14**, 20 (2020).
7. Hancock, F. *et al.* Metastability as a candidate neuromechanistic biomarker of schizophrenia pathology. *PLoS One* **18**, e0282707 (2023).
8. Hancock, F. *et al.* Metastability demystified — the foundational past, the pragmatic present and the promising future. *Nat. Rev. Neurosci.* **26**, 82–100 (2025).
9. Deco, G., Tagliazucchi, E., Laufs, H., Sanjuán, A. & Kringelbach, M. L. Novel Intrinsic Ignition Method Measuring Local-Global Integration Characterizes Wakefulness and Deep Sleep. *eNeuro* **4**, ENEURO.0106-17.2017 (2017).
10. Metzner, C. *et al.* Exploring global and local processes underlying alterations in resting-state functional connectivity and dynamics in schizophrenia. *Front. Psychiatry* **15**, 1352641 (2024).
11. Woodward, N. D., Rogers, B. & Heckers, S. Functional resting-state networks are differentially affected in schizophrenia. *Schizophr. Res.* **130**, 86–93 (2011).
12. Du, Y. *et al.* Interaction among subsystems within default mode network diminished in schizophrenia patients: A dynamic connectivity approach. *Schizophr. Res.* **170**, 55–65 (2016).
13. Sendi, M. S. E. *et al.* Aberrant Dynamic Functional Connectivity of Default Mode Network in Schizophrenia and Links to Symptom Severity. *Front. Neural Circuits* **15**, 649417 (2021).
14. Kottaram, A. *et al.* Brain network dynamics in schizophrenia: Reduced dynamism of the default mode network. *Hum. Brain Mapp.* **40**, 2212–2228 (2019).
15. Andrews-Hanna, J. R., Reidler, J. S., Sepulcre, J., Poulin, R. & Buckner, R. L. Functional-Anatomic Fractionation of the Brain's Default Network. *Neuron* **65**, 550–562 (2010).
16. Berna, F. *et al.* A Meta-Analysis of Autobiographical Memory Studies in Schizophrenia Spectrum Disorder. *Schizophr. Bull.* sbv099 (2016) doi:10.1093/schbul/sbv099.
17. Hill, M. O. Diversity and Evenness: A Unifying Notation and Its Consequences. *Ecology* **54**, 427–432 (1973).
18. Dice, L. R. Measures of the Amount of Ecologic Association Between Species. *Ecology* **26**, 297–302 (1945).
19. Rolls, E. T., Cheng, W. & Feng, J. Brain dynamics: the temporal variability of connectivity, and differences in schizophrenia and ADHD. *Transl. Psychiatry* **11**, 70 (2021).
20. Farinha, M., Amado, C., Morgado, P. & Cabral, J. Increased Excursions to Functional Networks in Schizophrenia in the Absence of Task. *Front. Neurosci.* **16**, 821179 (2022).

21. Wang, D. *et al.* Altered temporal, but intact spatial, features of transient network dynamics in psychosis. *Mol. Psychiatry* **26**, 2493–2503 (2021).

22. Holt, D. J. *et al.* An Anterior-to-Posterior Shift in Midline Cortical Activity in Schizophrenia During Self-Reflection. *Biol. Psychiatry* **69**, 415–423 (2011).

23. Spreng, R. N. *et al.* The default network of the human brain is associated with perceived social isolation. *Nat. Commun.* **11**, 6393 (2020).

24. Saris, I. M. J. *et al.* Social dysfunction is transdiagnostically associated with default mode network dysconnectivity in schizophrenia and Alzheimer's disease. *The World Journal of Biological Psychiatry* **23**, 264–277 (2022).

25. Subramaniam, K. *et al.* Computerized Cognitive Training Restores Neural Activity within the Reality Monitoring Network in Schizophrenia. *Neuron* **73**, 842–853 (2012).

26. American Psychiatric Association. *American Psychiatric Association. Diagnostic and Statistical Manual of Mental Disorders: DSM-5-TR. 5th Ed, Text Rev*. (2022).

27. Lobo, A., Ezquerra, J., Gómez Burgada, F., Sala, J. M. & Seva Díaz, A. Cognocitive mini-test (a simple practical test to detect intellectual changes in medical patients). *Actas Luso. Esp. Neurol. Psiquiatr. Cienc. Afines* **7**, 189–202 (1979).

28. von Elm, E. *et al.* The Strengthening the Reporting of Observational Studies in Epidemiology (STROBE) Statement: Guidelines for Reporting Observational Studies. *PLoS Med.* **4**, e296 (2007).

29. Ashburner, J. & Friston, K. J. Unified segmentation. *Neuroimage* **26**, 839–851 (2005).

30. Tzourio-Mazoyer, N. *et al.* Automated Anatomical Labeling of Activations in SPM Using a Macroscopic Anatomical Parcellation of the MNI MRI Single-Subject Brain. *Neuroimage* **15**, 273–289 (2002).

31. Thomas Yeo, B. T. *et al.* The organization of the human cerebral cortex estimated by intrinsic functional connectivity. *J. Neurophysiol.* **106**, 1125–1165 (2011).

32. Kuramoto, Y. *Chemical Oscillations, Waves, and Turbulence*. *Springer Series in Synergetics* (Springer Berlin Heidelberg, 1984). doi:10.1007/978-3-642-69689-3.

33. Shanahan, M. Metastable chimera states in community-structured oscillator networks. *Chaos: An Interdisciplinary Journal of Nonlinear Science* **20**, 013108 (2010).

34. Escrichs, A. *et al.* Characterizing the Dynamical Complexity Underlying Meditation. *Front. Syst. Neurosci.* **13**, 27 (2019).

35. Phipson, B. & Smyth, G. K. Permutation P-values Should Never Be Zero: Calculating Exact P-values When Permutations Are Randomly Drawn. *Stat. Appl. Genet. Mol. Biol.* **9**, (2010).

36. Winkler, A. M., Ridgway, G. R., Webster, M. A., Smith, S. M. & Nichols, T. E. Permutation inference for the general linear model. *Neuroimage* **92**, 381–397 (2014).

37. Holm, S. A simple sequentially rejective multiple test procedure. *Scandinavian Journal of Statistics* **6**, 65–70 (1979).

38. Efron, B. Better Bootstrap Confidence Intervals. *J. Am. Stat. Assoc.* **82**, 171–185 (1987).

Supplementary Files

This is a list of supplementary files associated with this preprint. Click to download.

- SupplementarymaterialSCIReport.docx